2

Multimodal Range Image Segmentation

Michal Haindl & Pavel Žid
Institute of Information Theory and Automation, Academy of Sciences CR
Czech Republic

1. Introduction

Computer vision is an area of the computer science which aims to make computers to have some functions owned by human vision system. During the research on computer vision, we often think about "how human see". Obviously, when a human observer views a scene, the observer sees not the whole complex scene, but rather a collection of objects. A common experience of segmentation is the way that an image can resolve itself into a figure, typically the significant, important object, and a ground, the background on which the figure lies.
The capability of human beings to segment the complex scene into separated objects is so efficient that we regard it as a mystery. At meantime, it appeals the researchers of computer vision who want to let computer have the same capability. So the task, Image Segmentation, is presented.
The chapter describes new achievements in the area of multimodal range and intensity image unsupervised segmentation. This chapter is organized as follows. Range sensors are described in section 2 followed by the current state of art survey in section 3. Sections 4 to 6 describe our fast range image segmentation method for scenes comprising general faced objects. This range segmentation method is based on a recursive adaptive probabilistic detection of step discontinuities (sections 4 and 5) which are present at object face borders in mutually registered range and intensity data. Detected face outlines guides the subsequent region growing step in section 6 where the neighbouring face curves are grouped together. Region growing based on curve segments instead of pixels like in the classical approaches considerably speed up the algorithm. The exploitation of multimodal data significantly improves the segmentation quality. The evaluation methodology a range segmentation benchmarks are described in section 7. Following sections show our experimental results of the proposed model (section 8), discuss its properties and conclude (section 9) the chapter.

1.1 Image Segmentation

There is no single standard approach to segmentation. The definition of the goal of segmentation varies according to the type of the data and the application type. Different assumptions about the nature of the images being analyzed lead to use of different algorithms. One possible image segmentation definition is: "Image Segmentation is a process of partitioning the image into non-intersecting regions such that each region is homogeneous and the union of no two adjacent regions is homogeneous" (Pal & Pal, 1993).

Source: Vision Systems: Segmentation and Pattern Recognition, ISBN 987-3-902613-05-9,
Edited by: Goro Obinata and Ashish Dutta, pp.546, I-Tech, Vienna, Austria, June 2007

The segmentation process is perhaps the most important step in image analysis since its performance directly affects the performance of the subsequent processing steps in image analysis and it significantly determines the resulting image interpretation. Despite its utmost importance, segmentation still remains as an unsolved problem in the general sense as it lacks a general mathematical theory. The two main difficulties of the segmentation problem are its underconstrained nature and the lack of definition of the "correct" segmentation. Perhaps as a consequence of these shortcomings, a plethora of segmentation algorithms has been proposed in the literature. These algorithms range from simple ad hoc schemes to more sophisticated ones using object and image models.
The area of segmentation algorithms typically suffers with the lack of benchmarking results and methodologies. With few rare exceptions in specific narrow applications single segmentation algorithm cannot be ranked and potential user has to experimentally validate several segmentation algorithms for his particular application.

1.2 Range Image Segmentation

Range images store, instead of brightness or colour information, the depth at which the ray associated with each pixel first intersects the object observed by a camera. In a sense, a range image is exactly the desired output of stereo, motion, or other shape-from vision modules. It provides geometric information about the object independent of the position, direction, and intensity of light sources illuminating the scene, or of the reflectance properties of that object.
Range image segmentation has been an instrument of computer vision research for nearly 30 years. Over that period several partial results have found its way into many industrial applications such as geometric inspection, reverse engineering or autonomous navigation systems. However similarly as in the spectral image segmentation area the range image segmentation problem is still far from being satisfactory solved.

2. Range Sensors

Range sensors can be grouped into the passive and active once. A rich variety of passive stereo vision techniques produce three-dimensional information. Stereo vision involves two processes: the binocular fusion of features observed by the two cameras and the reconstruction of their three dimensional preimage. An alternative to classical stereo is the photometric stereo (Horn, 1986). Photometric stereo is a monocular 3-D shape recovery method assuming single illumination point at infinity, Lambertian opaque surface and known camera parameters, that relies on a few images (minimally 3) of the same scene taken under different lighting conditions. If this before mentioned knowledge is not available, i.e., uncalibrated stereo, more intensity images are necessary. There are usually two processing steps: First, the direction of the normal to the surface is estimated at each visible point. The set of normal directions, also known as the needle diagram, is then used to determine the 3-D surface itself. At the limit, shape from shading requires a single image, but then solving for the normal direction or 3-D location of any point requires integration of data from all over the image.
Active sensing techniques promise to simplify many tasks and problems in machine vision. Active range sensing operates by illuminating a portion of the surface under controlled conditions and extracting a quantity from the reflected light (angle of return in

triangulation, time/phase/frequency delay in time of flight sensors) in order to determine the position of the illuminated surface area. This position is normally expressed in the form of a single 3-D point.

An active range sensor - a range camera - is a device which can acquire a raster (two-dimensional grid, or image) of depth measurements, as measured from a plane (orthographic) or single point (perspective) on the camera (Forsyth & Ponce, 2003). In an intensity image, the greyscale or colour of imaged points is recorded, but the depths of the points imaged are ambiguous. In a range image, the distances to points imaged are recorded over a quantized range. For display purposes, the distances are often coded in greyscale, usually that the darker a pixel is, the closer it is to the camera.

Intensity Image Range Image

Fig. 1. Example of registered intensity and range image

2.1. Triangulation Based (Structured Light) Range Sensors

Triangulation based range finders date back to the early seventies. They function along the same principles as passive stereo vision systems, one of the cameras being replaced by a source of controlled illumination (structured light). For example, a laser and a pair of rotating mirrors may be used to sequentially scan a surface. In this case, as in conventional stereo, the position of the bright spot where the laser beam strikes the surface of interest is found as the intersection of the beam with the projection ray joining the spot to its image. Contrary to the stereo case, however, the laser spot can normally be identified without difficulty since it is in general much brighter than the other scene points (in particular when a filter tuned to the laser wavelength is inserted in front of the camera), altogether avoiding the correspondence problem.

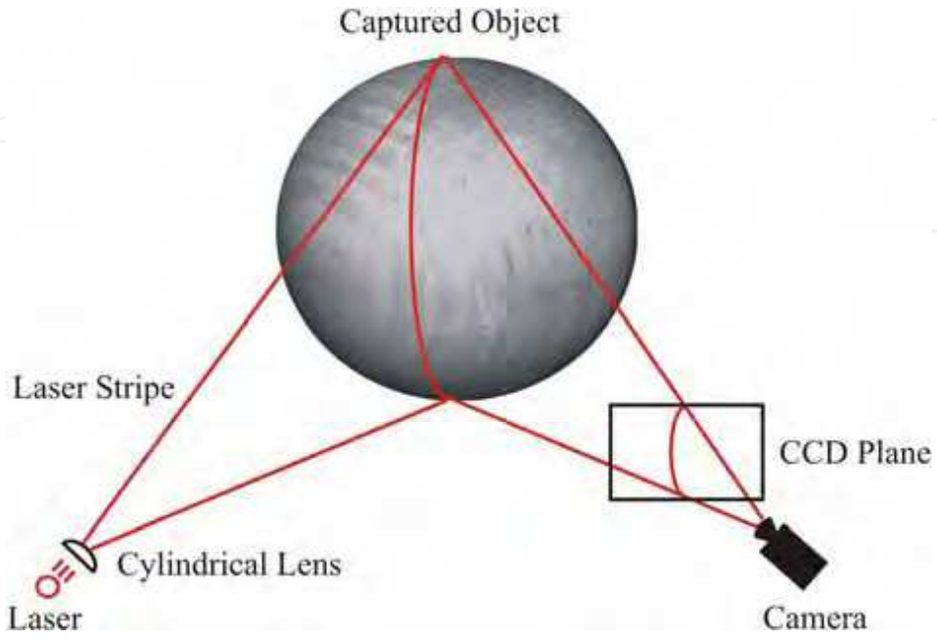

Fig. 2. Optical triangulation using laser beam for illumination.

Alternatively, the laser beam can be transformed by a cylindrical lens into a plane of light (Fig. 2.). This simplifies the mechanical design of the range finder since it only requires one rotating mirror. More importantly, perhaps, it shortens the time required to acquire a range image since a laser stripe, the equivalent of a whole image column, can be acquired at each frame.

A structured light scanner uses two optical paths, one for a CCD sensor and one for some form of projected light, and computes depth via triangulation. ABW GmbH and K2T Inc. are two companies which produce commercially available structured light scanners. Both of these cameras use multiple images of striped light patterns to determine depth. two example structured light patterns used by the K2T GRF-2 range camera are shown in Fig. 3.

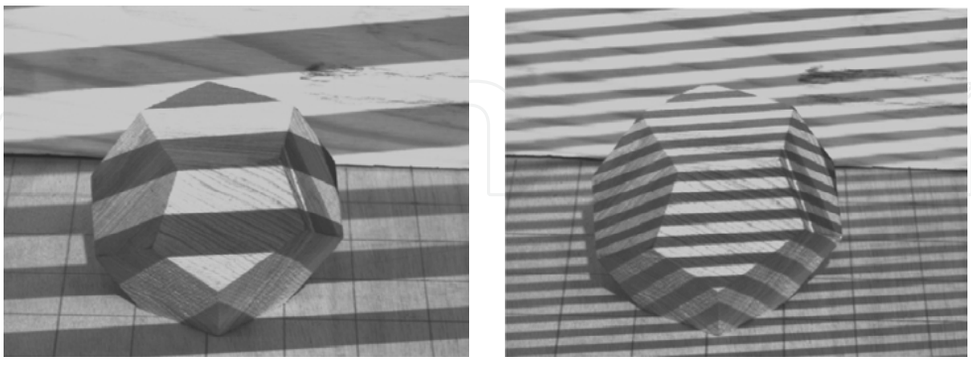

Fig. 3. Example images of two of the eight structured light patterns used by the K2T GRF-2 range camera.

Variants of these techniques include using multiple cameras to improve measurement accuracy and exploiting (possibly time coded) two dimensional light patterns to improve data acquisition speed. The main drawbacks of the active triangulation technology are relatively low acquisition speed and missing data at parts of the scene visible to the CCD sensor and not visible to the light projector. The resulting pixels in the range image, called shadow pixels, do not contain valid range measurements. Next difficulties arise from missing or erroneous data due to specularities. It is actually common to all active ranging techniques: a purely specular surface will not reflect any light in the direction of the camera unless it happens to lie in the corresponding mirror direction. Worse, the reflected beam may induce secondary reflections giving false depth measurements.

2.2. Time of Flight Range Sensors

The second main approach to active ranging involves a signal transmitter, a receiver, and electronics for measuring the time of flight of the signal during its round trip from the range sensor to the surface of interest (Dubrawski & Sawwa, 1996). This is the principle used in the ultrasound domain by the Polaroid range finder, commonly used in autofocus cameras from that brand and in mobile robots, despite the fact that the ultrasound wavelength band is particularly susceptible to false targets due to specular reflections. Time of flight laser range finders are normally equipped with a scanning mechanism, and the transmitter and receiver are often coaxial, eliminating the problem of missing data common in triangulation approaches. There are three main classes of time of flight laser range sensors:

- pulse time delay RS
  Pulse time delay sensor emits very brief, very intense pulses of light. The amount of time the pulse takes to reach the target and return is measured and converted to a distance measurement. The accuracy of these sensors is typically limited by the accuracy with which the time interval can be measured, and the rise time of the laser pulse.

- AM phase-shift RS
  AM phase-shift range finders measure the phase difference between the beam emitted by an amplitude-modulated laser and the reflected beam (see Fig. 4.), a quantity proportional to the time of flight.

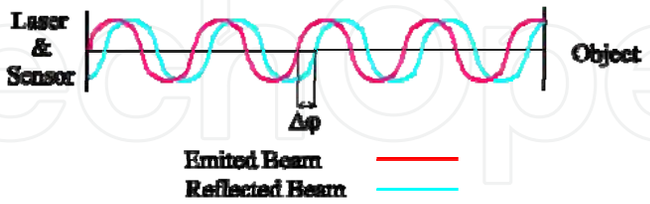

Fig. 4. Illustration of AM phase-shift range sensor measurement.

Measured distance *r* can be expressed as:

$$r = \Delta\varphi * \frac{\lambda_m}{4\pi} \quad (1)$$

where $\Delta\varphi$ is the phase difference between emitted and reflected beam and λ_m is the wave-length of modulated function. Due to periodical nature of modulated function the measurement is possible only in an ambiguity interval $r_a=\lambda_m/2$.

- FM beat RS
  FM beat sensors measure the frequency shift (or beat frequency) between a frequency-modulated laser beam and its reflection (see Fig. 5.), another quantity proportional to the round trip flight time.

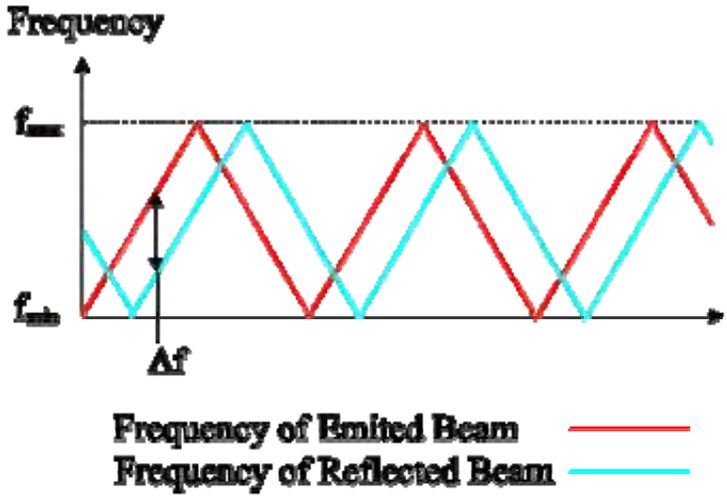

Fig. 5. Illustration of FM beat range sensor measurement.

Measured distance r can be expressed as:

$$r = c * \frac{f_b}{f_m * \Delta f}, f_b = |f_e - f_r| \tag{2}$$

where c is speed of light, f_m mean modulation frequency, Δf the difference between highest and lowest frequency in modulated run, f_e emitted beam frequency and f_r reflected beam frequency.

Time of flight range finders face the same problems as any other active sensors when imaging specular surfaces. They can be relatively slow due to long integration time at the receiver end. The speed of pulse time delay sensors is also limited by the minimum resolvable interval between two pulses. Compared to triangulation based systems, time of flight sensors have the advantage of offering a greater operating range (up to tens of meters), which is very valuable in outdoor robotic navigation tasks.

3. State of the Art

There are many spectral image segmentation algorithms published in computer vision literature and a number of good survey articles (Besl & Jain, 1985), (Sinha & Jain, 1994) is available but substantially less range image segmentation algorithms were published. Mutual comparison of their segmentation quality and performance is very difficult because of lack of sound experimental evaluation results. A rare exception in the area of planar face objects range segmentation is published in (Hoover et al., 1996a) together with experimental data available on their Internet server. Because this evaluation methodology became de facto standard in the area of planar range segmentation algorithms comparison, these data and results are used also for our algorithm evaluation.

3.1. Range Segmentation Principles

There are several methods for segmenting an image into regions, which, subsequently, can be analyzed, based on their shapes, sizes, relative positions, and other characteristics, and there are several possible categorizations of segmentation techniques. The most common categorization accepted also in this chapter sorts segmentation methods into three or four different philosophical perspectives. We name them after the terminology "pixel based segmentation, edge based segmentation, region based segmentation and hybrid segmentation".

3.1.1. Pixel Based Segmentation

Pixel based segmentation is the most local method to address the task of image segmentation. Every pixel has to be sorted to some certain class. At last, the pixels belonging to the same class which are contiguous will constitute one segmented region.

3.1.2. Edge Based Segmentation

Edge based segmentation is more global than pixel based segmentation, but it is more local when compared to the area based segmentation. So it is on the "middle level".
Edge based segmentation make use of the clue that "how human see" for the second time, because a person always has the principle that there is an edge in some certain sense between two segmentable objects (Zhang & Zhao, 1995), (Palmer et al., 1996). An edge pixel is characterized by a vector that shows a particular position, size and direction of discontinuity. Sometimes only the size is determined. The "direction" of the edge is perpendicular to the "direction" of the rim of the object.

3.1.3. Region Based Segmentation

Among the four surveyed approaches, region based segmentation is the most global method. This approach groups pixels into regions based upon two criteria: proximity and homogeneity. Most region based methods produce these groupings either by splitting the image, or its regions, into smaller regions (Lee et al., 1998), merging small regions into larger ones (Hoover et al., 1996a), (Besl & Jain, 1988), or splitting and merging until the criteria are maximally satisfied (Haralick & Shapiro, 1985), (Chang, 1994), (Hijjatoleslami & Kittler, 1998). In two-dimensional region growing, regions that have pixels that are "four-connected" (Fig. 6.-left), that is, directly neighboring each other in any of the four horizontal and vertical directions, are considered to be in proximity to one another. Other region growing

algorithms extend these criteria to "eight-connected" pixels by also including the four diagonal directions (Fig. 6.-right).

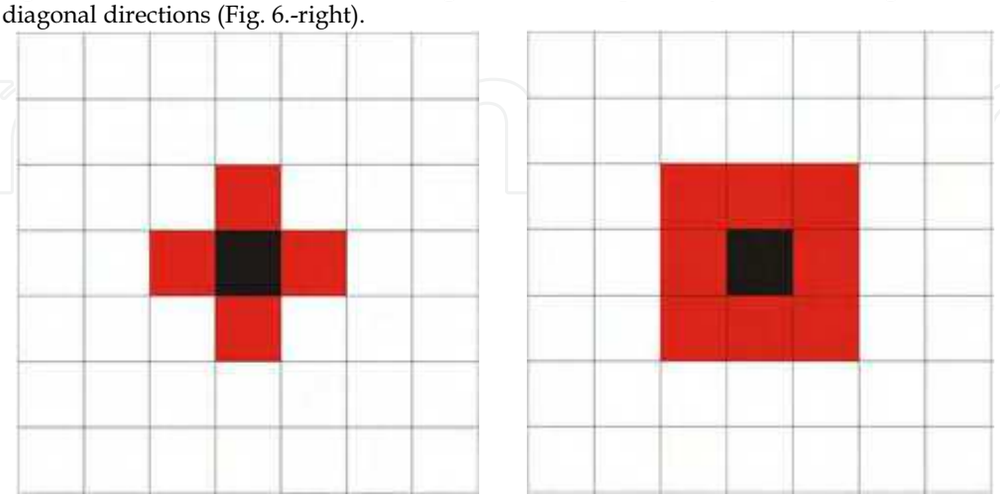

Four-Connected Neighbours & Eight-Connected Neighbours

Fig. 6. Neighbourhood examples.

The second criterion, homogeneity, is satisfied by an implementation specific function that quantifies the similarity between regions. This function may be based on a comparison of any single or combination of available region statistics .

3.1.4. Hybrid Segmentation

Hybrid techniques are trying to combine advantages of two or more previously described segmentation methods. They are expected to provide more accurate segmentation of images. Pavlidis et al. (Pavlidis & Liow, 1990) describe a method to combine segments obtained by using a region-growing approach, where the edges between regions are eliminated or modified based on contrast, gradient and shape of the boundary. Haddon and Boyce (Haddon & Boyce, 1990) generate regions by partitioning the image co-occurrence matrix and then refining them by relaxation using the edge information. Chu and Aggarwal (Chu & Aggarwal, 1993) present an optimization method to integrate segmentation and edge maps obtained from several channels, including visible, infrared, etc., where user specified weights and arbitrary mixing of region and edge maps are allowed. The method presented in this chapter can be classified as hybrid technique, because we use edge detection as the first step of the algorithm and segment based region growing as the second step.

3.2. Planar Face Segmentation Algorithms

A specially simplified range image segmentation task occurs when we may assume some additional prior information about the segmented scene. One of the most frequent assumptions is planarity of range scene objects faces. A planar surface can be characterized as a connected set of 3D surface points at which the two principal curvatures (alternatively, the Gaussian and mean curvatures) are zero. It gives the chance to simplify the model of the region and thus simplify the whole segmentation process.

3.2.1. The USF Range Segmentation Algorithm

This segmenter (Hoover et al., 1996a) works by computing a planar fit for each pixel and then growing regions whose pixels have similar plane equations. The pixel with the smallest interiorness measure is chosen as a seed point for region growing. The border of the region is recursively grown until no pixels join, at which time a new region is started using the next best available seed pixel (based on interiorness measure). Pixels are only allowed to participate in this process once. If a region's final size is below a threshold, then the region is discarded. This algorithm shows good segmentation results over test sets especially in under-segmentation measure and has only 5 parameters, but it is discriminated by its computational speed.

3.2.2. The WSU Range Segmentation Algorithm

The WSU range image segmentation method (Hoffman & Jain, 1987), (Flynn & Jain, 1991) is not optimized for polyhedral objects but can accommodate natural quadric surfaces as well. It was modified to accept only first-order surface fits, but no other special steps were taken to exploit the planar nature of the scenes. Prior to any processing, the range points are uniformly scaled to fit within a 5×5 cube. Than jump edge pixels are identified. Surface normals are estimated at each range pixel with no jump edges in a neighbourhood. The six-dimensional image is formed by concatenating the estimated surface normals to their corresponding pixels.

These 6-vectors are fed to a squared-error clustering algorithm, which finds groupings in the data set based on similarity between the data points. Since these points reflect both position and orientation, the tendency is to produce clustering consisting of connected image subsets, with pixels in each cluster having similar orientation. The selected clustering is converted into an image segmentation by assigning each range pixel to the closest cluster centre in the clustering. A further merging step joins segments if they are adjacent and have similar parameters. This algorithm achieved the worst result in all segmentation quality measures among the four compared algorithms. The next drawback of this algorithm is high number of tuneable parameters and relatively high computational times.

3.2.3. The UBP range segmentation algorithm

This segmenter (Jiang & Bunke, 1994) is based on the fact that, in the ideal case, the points on a scan line that belong to a planar surface form a straight 3D line segment. On the other hand, all points on a straight 3D line segment surely belong to the same planar surface. Therefore, they first divide each scan line into straight line segments and subsequently perform a region growing process using the set of line segments instead of the individual pixels.

A potential seed region for region growing is a triple of line segments on three neighbouring scan lines. The candidate with the largest total line segment length is chosen as the optimal seed region. In the subsequent region growing process, a line segment is added to the region if the perpendicular distance between its two end points and the plane equation of the region is within a dynamic threshold. This process is repeated until no more line segments can be added, at which time a new region is started using the next best available seed region. If a region's final size is below a threshold, then the region is discarded. This algorithm is probably the best one of all methods surveyed in (Hoover et al., 1996a). It achieves high number of correctly detected region over both test sets, low number of

undersegmented regions, but it oversegments some regions. The number of parameters is relatively high. This is the fastest algorithm surveyed in (Hoover et al., 1996a).

3.2.4. The UE Range Segmentation Algorithm

The UE segmentation algorithm (Hoover et al., 1996a) is a region growing type of algorithm along the lines of the USF segmenter. Initial surface normals are calculated at each pixel using a plane fit to the data. Depth and normal discontinuity detection is performed using simple thresholds between neighbouring pixels. Gaussian (H) and mean (K) curvature are estimated at each pixel. Pixels can be labelled as belonging to particular surface types based on the combined signs of the (H, K) values. Once each pixel is labelled properly with the signs of H and K, any eight--connected pixels of similar labelling are grouped to form initial regions. This segmentation map is then morphologically dilated and eroded in a specifiable manner to fill small Unknown areas, remove small regions, and separate thinly connected components. For each region in the initial segmentation above a minimal size a least squares surface fitting is performed. Then each region in turn is grown. The UE segmenter obtains slightly better measures of correct detection than does the UBP segmenter but the difference in processing speeds is noteworthy. The main drawback of this algorithm is high number of its parameters. Nearly a dozen values should be adjusted before the segmentation.

3.2.5. Robust Adaptive Segmentation (ALKS) Algorithm

The authors of this method (Lee et al., 1998) proposed an image segmentation technique using the robust, adaptive least *k*th order squares (ALKS) estimator which minimizes the *k*th order statistics of the squared of residuals. The optimal value of *k* is determined from the data, and the procedure detects the homogeneous surface patch representing the relative majority of the pixels. The method defines the region to be processed as the largest connected component of unlabelled pixels. Applies the ALKS procedure to the selected region and discriminates the inliers, labels the largest connected component of inliers as the delineated homogeneous patch and refines the model parameter estimates by a least--squares fit to the inliers. Than it repeats these steps until the size of the largest connected component is less than a threshold. To eliminate the isolated outliers surrounded by inliers an unlabelled pixel is allocated to the class of the majority of its labelled four-connected neighbours. For this method we can only compare results published in the article (Lee et al., 1998). These results show that the ALKS method tends to undersegment some faces. We have no information about computational times for this method.

3.2.6. Segmentation through the integration of different strategies (PPU)

The authors of this paper (Bock & Guerra, 2001) consider the problem of segmenting range images into planar regions.

The approach they present combines different strategies for grouping image elements to estimate the parameters of the planes that best represent the range data. The strategies differ not only in the way candidate planes are hypothesized but also in the objective function used to select the best plane among the potential candidates. The method they consider integrates in an effective way different strategies for plane recovery. There are mainly three procedures all based on random sampling. Three main procedures are invoked sequentially in a given order for new plane detection in iteration, the next one executed only when the previous ones do not detect a significant plane. Once the parameters of the best plane are

found at a given iteration, the plane is expanded over the entire image and all the fragments of the same surface in the image are labelled as belonging to the same plane. This method achieved the worst result in the comparison.

3.2.7. The OU segmentation algorithm

The segmentation algorithm OU (Jiang et al., 2000) is based on the analysis of intersection of the scene by arbitrary planes. At first, the range image is divided into two hemi-spaces by an imaginary plane, and then it binarizes each pixel on the range image. On that image, the issue of plane detection is turned into edge detection on the binary image. Authors applied Hough transform for derivative image to do it, because test images contain much noise. The topological information in the binary image can also be used for end-point determination and grouping detected line segments. The imaginary plane is translated step by step and the set of line segments is obtained. To accelerate this algorithm, the voting space for Hough transform is limited using information of prior line detection. Then planes are made by grouping line segments: If two lines share a plane, the lines are parallel to each other and have a close distance. Therefore all line segments are classified into several groups using gradient, distance and arrangement of end--points of the lines. The topological cue of binary image can be also exploited. Finally the range image is filled by polygons which are generated from two neighbouring lines. Against the case of fragmentation of polygons the normal vectors of each planar surface are evaluated and unified if the difference of normal vectors of neighbouring planar surfaces is small enough.

3.2.8. The UA segmentation algorithm

The segmentation algorithm UA (Jiang et al., 2000 performs a fast hierarchical processing in a multiresolution pyramid, or quadtree, based on (Loke & duBuf, 1998) and (Wilson & Spann, 1988). It must be noted that the method has only very recently been adapted for range images. Its current disadvantage is the information loss which is caused by linearly combining the components of the surface normal vector. A quadtree of L levels is built with at the base (level 0) the original range image on a regular grid. Low-resolution depth data at each higher level are determined by a low-pass filtering of depths at the lower level in no overlapping blocks of size 2×2. This reduces the noise, allowing the estimation of accurate normal vectors at the highest level $L - 1$. New filter technique is applied in order to increase the homogeneity of the data and to reduce the noise. At level $L - 1$, data clusters are determined using the local-centroid algorithm (Wilson & Spann, 1988). Thereafter, the segmentation at level $L - 1$ is obtained by setting each pixel to the label of its nearest cluster. Starting at level $L - 1$ and ending at level 1, the segmentation at each lower level is obtained by refining the boundary. At level 0, a component labelling is performed, because the segmentation may contain regions which have the same label, but which are not spatially connected. All regions smaller than a minimum region size are disregarded.

3.3. Non-Planar Face Segmentation Algorithms

If the measured range scene contains general objects and we cannot use the simplifying planar face assumption, the segmentation task is substantially more difficult. There is very few non-planar range segmentation algorithms published and no benchmarking methodology generally accepted.

3.3.1. The UBC Range Segmentation Algorithm

The UBC segmenter (Jiang & Bunke, 1998) consists of two parts: edge detection and grouping of edge points into closed regions. It makes use of the fact that each scan line (row, column or diagonal) of a range image is a curve in 3-D space. Therefore, it partitions each scan line into a set of curve segments by means of a splitting method. All the splitting points represent potential edges. The jump and crease edge strength of the edge candidates are evaluated by analytically computing the height difference and the angle between two adjacent curve segments, respectively. Each pixel can be assigned up to four edge strength values of each type (jump and crease) from the four scan lines passing through the pixel. These edge strength values are combined by taking the maximum to define the overall edge strength of each type. The grouping process is based on a hypochapter generation and verification approach. From the edge map, regions can be found by a component labelling. Due to the inevitable gaps in the edge chains, however, this initial grouping usually results in under-segmentation. To recognize the correctly segmented and under-segmented regions, a region test is performed for each region of the initial segmentation. If the region test is successful, the corresponding region is registered. Otherwise, the edge points within the region are dilated once, potentially closing the gaps. Then, hypochapter generation (component labelling) and verification (region test) are carried out for the region. This process is recursively done until the generated regions have been successfully verified or they are no longer considered because of too small a region size. The results suggest that the UBC segmentation algorithm substantially out-performs the BJ algorithm. However, these results should be interpreted carefully. The UBC segmenter has a fundamental limitation. The edge detection method described above is able to detect jump and crease edges but not smooth edges (discontinuities only in curvature). This seems to be true for all edge detectors reported in the literature.

3.3.2. Variable Order Surface Fitting (BJ) Algorithm

Besl and Jain developed a segmentation algorithm (Besl & Jain, 1988) which uses signs of surface curvature to obtain a coarse segmentation and iteratively refines it by fitting bivariate polynomials to the surfaces. The algorithm begins by estimating the mean and Gaussian surface curvature at every pixel and uses the signs of the curvatures to classify each pixel as belonging to one of eight surface types. The resultant coarse segmentation is enhanced by an iterative region growing procedure. For every coarse region, a subregion of a size at or above a threshold is selected to be a seed region. Low order bivariate polynomials are used to produce an estimated surface fit to the seed region. Next, all pixels in all regions of the image that are currently outside the seed region are tested for possible inclusion into the current region. The largest connected region which is composed of pixels in the seed region and pixels that passes the compatibility tests is chosen as the new seed region. Expansion continues until either there is almost zero change in region size since the last iteration, or when the surface fitting error becomes larger than a threshold. Finally, fit error is calculated, and if it falls below a threshold the region is accepted. If not, the region is rejected and the seed region that produced it is marked off so that it may not be used again.

3.3.3. Industrial Research Limited Simple Surface Segmentation (IRLBC and IRLRG)

The authors of this paper (McIvor et al., 1997) described a method for the recognition of simple curved surface patches from dense 3--D range data, such as that provided by a

structured light system. Patches from planes, spheres, cylinders, and ruled surfaces are considered. The approach can be summarised as follows. The first step is to estimate the local surface geometry (the principal quadric) at each visible surface point. Then points at which the signs of the Gaussian and mean curvatures are inconsistent with those of a particular surface type are rejected from further consideration. Each remaining point is mapped to a point in the parameter space of the surface type. By using an unsupervised Bayesian classification (IRLBC method) or region growing algorithm (IRLRG method), the clusters in parameter space that correspond to surface patches are identified, and the parameters of that surface can be determined.

4. Multimodal Range Image Segmentation

4.1. Face Outline Detection

We assume mutually registered range $(y_{t,r})$ and intensity $(y_{t,i})$ data $Y_t = [y_{t,r}, y_{t,i}]^T$ of the scene to be modeled in the unshaded part (scene part with valid range measurements) by an adaptive causal simultaneous autoregressive model (SAR) in some chosen direction:

$$Y_t = \gamma Z_t + \varepsilon_t \tag{3}$$

Where $\gamma = [A_1, \ldots, A_\eta]$ is the $2 \times \eta$ unknown parameter matrix and η = card I_t. We denote the $2\eta \times 1$ data vector $Z_t = [Y_{t-i}^T : \forall i \in I_t]$ with a multi-index $t = (m,n)$; m, n are the row and column indices, respectively. The multiindex changes according to chosen direction of movement on the image plane e.g. $t\text{-}1 = (m,n\text{-}1)$, $t\text{-}2 = (m,n\text{-}2), \ldots, I_t$ is some contextual causal or unilateral neighbour index shift set. The white noise vector ε_t has zero mean and constant but unknown covariance matrix Ω. We further assume uncorrelated noise vector components, i.e., $E\{\varepsilon_{t,r}\ \varepsilon_{t,i}\} = 0\ \forall t$ and the probability density of ε_t to have the normal distribution independent of previous data and being the same for every time t. The task consists in finding the conditional prediction density $p(Y_t \mid Y^{(t-1)})$ given the known process history $Y^{(t-1)} = \{Y_{t-1}, Y_{t-2}, \ldots, Y_1, Z_t, Z_{t-1}, \ldots, Z_1\}$ and taking its conditional mean estimation $\hat{Y}$ for the predicted data. If the prediction error is greater than an adaptive threshold the algorithm assumes an object face edge pixel.

Assuming normality of the white noise component ε_t, conditional independence between pixels and the normal-Wishart parameter prior, we have shown (Haindl & Šimberová, 1992) that the conditional mean value is:

$$\hat{Y}_t = E\left[Y_t \middle| Y^{(t-1)}\right] = \hat{\gamma}_{t-1} Z_t \tag{4}$$

The following notation is used in (4):

$$\hat{\gamma}_{t-1} = V_{zz(t-1)}^{-1} V_{zy(t-1)}$$

$$V_{t-1} = \hat{V}_{t-1} + V_0$$

$$\hat{V}_{t-1} = \begin{pmatrix} \hat{V}_{yy(t-1)} & \hat{V}_{zy(t-1)}^T \\ \hat{V}_{zy(t-1)} & \hat{V}_{zz(t-1)} \end{pmatrix}$$

$$\hat{V}_{xw(t-1)} = \alpha \hat{V}_{xw(t-2)} + X_{t-1} W_{t-1}^T$$

and V_0 is a positive definite matrix. We assume slowly changing parameters, consequently these equations were modified using a constant exponential "forgetting factor" α to allow parameter adaptation. It is easy to check (see (Haindl & Šimberová, 1992)) also the validity of the following recursive parameter estimator:

$$\hat{\gamma}_t = \hat{\gamma}_{t-1} + (\alpha^2 + Z_t^T V_{zz(t-1)}^{-1} Z_t)^{-1} V_{zz(t-1)}^{-1} Z_t (Y_t - \hat{\gamma}_{t-1}^T Z_t)^T \tag{5}$$

Let us define the following three conditions with adaptive thresholds (7),(8):

$$Y_t \notin S \tag{6}$$

$$\left| \hat{y}_{t,r} - y_{t,r} \right| > \frac{2.5}{l} \sum_{j=1}^{l} \left| \hat{y}_{t-j,r} - y_{t-j,r} \right| \tag{7}$$

$$\left| \hat{y}_{t,i} - y_{t,i} \right| > \frac{2.5}{l} \sum_{j=1}^{l} \left| \hat{y}_{t-j,i} - y_{t-j,i} \right| \tag{8}$$

where S is the shaded (unmeasured part) of the range image. The pixel t is classified as an object edge pixel (a detected step discontinuity pixel) iff either the conditions (6),(7) or (6), non (7),(8) hold. Both adaptive thresholds are proportional to the local mean prediction error estimation.

4.2. Competing Models

Let us assume two SAR models (3) M_1 and M_2 with the same number of unknown parameters ($\eta_1 = \eta_2 = \eta$) and an identical neighbour index shift sets $I_{t'}$. They differ only in their forgetting factors $\alpha_1 > \alpha_2$. The model M_1, $\alpha_1 \approx 1$ represents homogeneous image areas while the second model better represents new information coming from crossing some face borders because it allows quicker adaptation to this new information. The optimal decision rule for minimizing the average probability of decision error chooses the maximum a posterior probability model, i.e. a model whose conditional probability given the past data is the highest one. Predictors used in the presented algorithm can be therefore completed as:

$$\hat{Y}_t = \begin{cases} \hat{\gamma}_{1,t-1} Z_t, & if\ (10)\ holds \\ \hat{\gamma}_{2,t-1} Z_t, & otherwise \end{cases} \tag{9}$$

where Z_t is a data vector identical to both models and

$$p(M_1 \left| Y^{(t-1)} \right.) > p(M_2 \left| Y^{(t-1)} \right.) \tag{10}$$

The analytical solution has the following form (Haindl & Šimberová, 1992):

$$p(M_i|Y^{(t-1)}) = k\Gamma\left(\frac{\psi(t-1)-\eta+2}{2}\right)\left|V_{i,zz(t-1)}\right|^{-\frac{1}{2}}\lambda_{i,t-1}^{-\frac{\psi(t-1)-\eta+2}{2}} \quad (11)$$

where k is a common constant. All statistics related to a model M_1 (6), (11) are computed using the exponential forgetting constant α_1 while symmetrical statistics of the model M_2 are computed using the second constant α_2.
The solution of (11) uses the following notations:

$$\psi(t) = \alpha^2\psi(t-1)+1 \quad (12)$$

$$\lambda_{t-1} = V_{yy(t-1)} - V_{zy(t-1)}^T V_{zz(t-1)}^{-1} V_{zy(t-1)} \quad (13)$$

The determinant $|V_{zz(t)}|$ as well as λ_t can be evaluated recursively (Haindl & Šimberová, 1992):

$$\left|V_{zz(t)}\right| = \left|V_{zz(t-1)}\right|\alpha_i^{2\eta}\left(1+Z_t^T V_{zz(t-1)}^{-1} Z_t\right)$$

$$\lambda_t = \lambda_{t-1}\alpha_i^2\left(1+\left(y_t - \hat{P}_{t-1}^T Z_t\right)^T \lambda_{t-1}^{-1}\left(y_t \hat{P}_{t-1}^T Z_t\right)\left(\alpha_i^2 + Z_t^T V_{zz(t-1)}^{-1} Z_t\right)^{-1}\right)$$

For numerical realization of the predictor (9) see discussion in (Haindl & Šimberová, 1992).

4.3. Face Detection

The previous step of the algorithm detects correct face outlines however some pixels on these edges can be either missing or edges can be incomplete. This missing information is estimated in a curve segment-based region growing process. Curves to be grown do not need to be of maximal length through the corresponding object face. Any curve segments can serve as initial estimation however longer curve segments speed up the region growing step. The only restriction imposed on them is that they are not allowed to cross face borders detected in the previous step of the algorithm. These curve segments can be generated in two mutually perpendicular directions but our current implementation uses only one of these directions.
A curve is represented using the cubic spline model:

$$Y_{r_i}^{s_i} = a_{s_i}(r_i - s_i)^3 + b_{s_i}(r_i - s_i)^2 + c_{s_i}(r_i - s_i) + d_{s_i}$$

for the interval $r_i \in \langle s_i; s_{i+\Delta}\rangle$, Δ=1 for the single-scale version of the algorithm, i=1 for columnwise or i=2 for rowwise direction, and r_j=s_j for $j \neq i$. Splines representing segments in a chosen direction are computed and parameter space Ξ is created over the image lattice. Two curve segments s_i,t_i in the same column (row) are merged together iff:

1. They have similar slope

$$\frac{\delta Y_{r_i}^{s_i}}{\delta r_i} \approx \frac{\delta Y_{r_i}^{t_i}}{\delta r_i}$$

The slope for identical steps Δ=1 is dependent on first three spline parameters, i.e.

$$\frac{\delta Y_{r_i}^{s_i}}{\delta r_i} = 3a_{s_i} + 2b_{s_i} + c_{s_i}$$

2. They have similar curvature

$$\frac{\delta^2 Y_{r_i}^{s_i}}{\delta r_i^2} \approx \frac{\delta^2 Y_{r_t}^{t_i}}{\delta r_i^2}$$

The curvature we approximate with the b_{Si} parameter

$$b_{s_i} = \frac{1}{2}\frac{\delta^2 Y_{r_i}^{s_i}}{\delta r_i^2}$$

Both conditions are satisfied if we require similar spline parameters a_{Si}, b_{Si}, c_{Si} for segments to be merged. The similarity measure chosen is the squared Euclidean distance. Similarly two parallel neighbouring curve segments r, ŕ r ∈ <s_i; s_i + 1> × r_j ŕ ∈ <s_i; s_i + 1> × (r_j + 1) are merged if they share similar parameters in their corresponding spline intervals (r_i). A fixed threshold we use in the current version depends on data; it has to be large enough to allow for parameters changes during a curved face following but simultaneously not too large to merge different faces together.

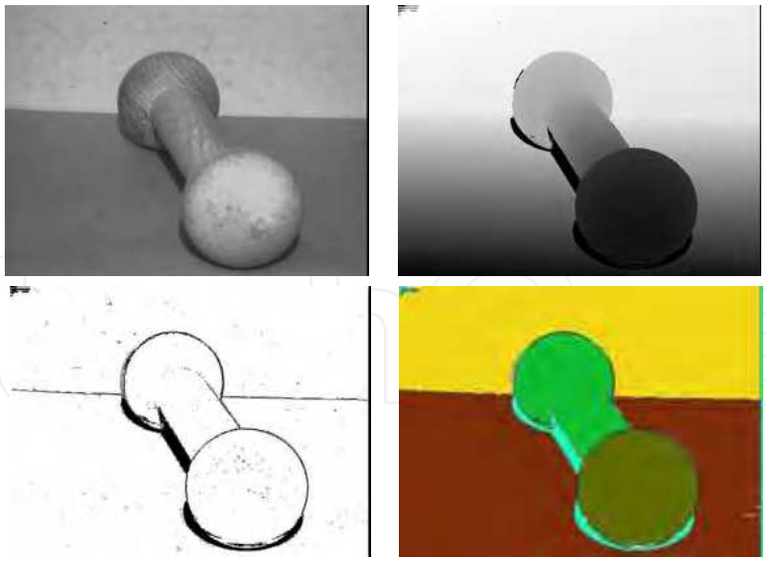

Fig. 7. Dumbbell intensity and range image, the combined edge map and the segmentation result.

5. Evaluation Methodology

For the segmentation quality evaluation we decided to use test data and methodology provided by (Hoover et al., 1996a) and (Hoover et al., 1996b) authors provided not only range image data, but the data together with ground truth segmentation of all images and a tool, which measures quality of segmentation results. Although no such experimental data can prove properties of a segmentation algorithm this set is large enough to suggest its expected behaviour and enables to rank the tested algorithm with some other previously published ones. Last but not least it is a rare world-wide accepted methodology for comparing planar face range image segmentation results.

The problem of image segmentation is a classical one and yet different definitions exist in the literature. Thus we begin by formally defining the problem we consider here. Let R represents the entire image region. We may view segmentation as a process that partitions R into n subregions R_1, R_2,…, R_n, such that

1. $\bigcup_{i=1}^{n} R_i = R$
2. R_i is a connected region, i=1,2,…,n
3. $R_i \cap R_j$ = 0 for all i and j, $i \neq j$
4. $Pred(R_i)$ = TRUE for i=1,2,…,n and
5. $Pred(R_i \cap R_j)$= FALSE for $i \neq j$

where $Pred(R_i)$ is a logical predicate over the points in set R_i and 0 is the empty set.

In some works the item 5 of this definition is modified to apply only to adjacent regions, as no bordering regions may well have the same properties, sometimes the item 2 is completely left out. Besides these inconsistencies, there are technical difficulties in using this definition for range image segmentation. Some range pixels do not contain accurate depth measurements of surfaces. This naturally leads to allowing non--surface pixels (areas), perhaps of various types. Regarding the above definition, non-surface areas do not satisfy the same predicate constraints (items 4 and 5) as regions that represent surfaces. It is also often convenient to use the same region label for all non-surface pixels in the range image, regardless of whether they are spatially connected. This violates item 2 of the above definition. Finally, we also require that the segmentation be 'crisp'. No sub pixel, multiple or 'fuzzy' pixel labelling are allowed. Comparison of machine segmentation (MS) of a range image to the ground truth (GT) is done as follows. Let M be the number of regions in the MS, and N be the number of regions in the GT. GT does not include any non-surface pixel areas. Similarly, MS does not include any pixels left unlabelled (or not assigned to a surface) by segmenter. Let the number of pixels in each machine-segmented region R_m (where m=1,…, M) be denoted P_M. Similarly, let the number of pixels in each ground truth region R_n (where n=1,…, N) be denoted P_n. Let $O_{mn} = R_m \cap R_n$ be the number of pixels of both regions R_m and R_n whose image coordinates occupy the same range in their respective images. Thus, if there is no overlap between the two regions, O_{mn} = 0, while if there is complete overlap, $O_{mn} = P_m = P_n$.

An $M \times N$ contingency table is created, containing O_{mn} for m=1,…, M and n=1,…, N. Implicitly attached to each entry are the percentages of overlap with respect to the size of each region. O_{mn}/P_m represents the percentage of m that the intersection of m and n covers.

Similarly, O_{mn}/P_n represents the percentage of n that the intersection of m and n covers. These percentages are used in determining region segmentation classifications.
We consider five types of region classification: **correct detection**, **over-segmentation**, **under-segmentation**, **missed** and **noise**. Over-segmentation, or multiple detections of a single surface, results in an incorrect topology. Under-segmentation, or insufficient separation of multiple surfaces, results in a subset of the correct topology and a deformed geometry. A missed classification is used when a segmenter fails to find a surface which appears in the image (false negative). A noise classification is used when the segmenter supposes the existence of a surface which is not in the image (false positive). Obviously, these metrics could have varying importance in different applications.
The formulas for deciding classification are based upon a threshold T, where $0.5 < T \leq 1.0$. The value of T can be set to reflect the strictness of definition desired. The following metrics define each classification:

1. An instance of a **correct detection** classification
   A pair of regions R_n in the GT image and R_m in the MS image are classified as an instance of correct detection if
   a) $O_{mn} \geq T \times P_m$ (at least T percent of the pixels in region R_m in then MS image are marked as pixels in region R_n in the GT image), and
   b) $O_{mn} \geq T \times P_n$ (at least T percent of the pixels in region R_n in then GT image are marked as pixels in region R_m in the MS image).

2. An instance of an **over-segmentation** classification
   A region R_n in the GT image and a set of regions in the MS image $R_{m1},\ldots,R_{mx}$, where $2 \leq x \leq M$, are classified as an instance of over-segmentation if
   a) $\forall\ i \in x, O_{mi\,n} \geq T \times P_m$ (at least T percent of the pixels in each region R_{mi} in the MS image are marked as pixels in region Rn in the GT image), and
   b) $\sum_{i=1}^{x} O_{mi\,n} \geq T \times P_n$ (at least T percent of the pixels in region R_n in the GT image are marked as pixels in the union of regions $R_{m1},\ldots, R_{mx}$ in the MS image).

3. An instance of an **under-segmentation** classification
   A set of regions in the GT image $R_{n1},\ldots, R_{nx}$, where $2 \leq x \leq M$, and a region R_m in the MS image are classified as any instance of under-segmentation if
   a) $\sum_{i=1}^{x} O_{mni} \geq T \times P_m$ (at least T percent of the pixels in region R_m in the MS image are marked as pixels in the union of regions $R_{n1},\ldots,R_{nx}$ in the GT image), and
   b) $\forall\ i \in x,\ O_{m\,ni} \geq T \times P_{ni}$ (at least T percent of the pixels in each region R_{ni} in the GT image are marked as pixels in region R_m in the MS image).

4. An instance of a **missed** classification
   A region R_n in the GT image that does not participate in any instance of correct detection, over-segmentation or under-segmentation is classified as missed.
5. An instance of a noise classification
   A region R_m in the MS image that does not participate in any instance of correct detection, over-segmentation or under-segmentation is classified as noise.

The authors of (Hoover et al., 1996a) created publicly available tool, which measures results of segmentation using described performance metrics. There are certainly many other possibilities how to compare segmentation results and some of them will result in different algorithms rating but above performance metrics is the only one which is generally accepted and hence enables mutual comparison of different published results.

6. Results

We tested the algorithm on a test set (Powel et al., 1998) of 39 range images from scenes containing planar, cylindrical, spherical, conical and toroidal object surfaces. This set was created by authors of (Powel et al., 1998) using a *K²T* structured light scanner model GRF-2. The scanner precision is 0.1 mm and data were quantized into a $640 \times 480 \times 8$ bit data space. Single scenes have between 1 to 120 surface patches of varying sizes. We compared our results Fig. 8. with three previously published methods (Besl & Jain, 1988), (Jiang & Bunke, 1998), (Haindl & Žid, 1998). As can be seen on Fig. 8. (colour version) our method outperforms these alternative methods. The average improvement over our previously published method (Haindl & Žid, 1998) in the correct segmentation criterion (Hoover et al., 1996) is 30%. Alternatively the results were evaluated also visually comparing range data segmentation results with corresponding intensity images (Figs. 7., 9.).
Visual comparison of the results demonstrates very good quality of detected borders using our algorithm. The borders are clean and accurately located. The segmentation algorithm properly found most required non-planar object surfaces in our test examples.

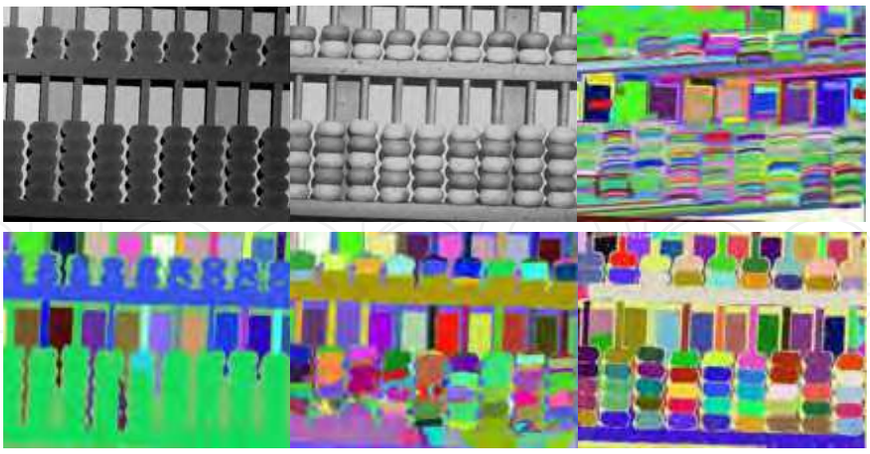

Fig. 8. Range, intensity measurements and the corresponding Besl & Jain (Besl & Jain, 1988) (upper row), UB (Jiang & Bunke, 1998), (Haindl & Žid, 1998) and the presented method abacus segmentation results.

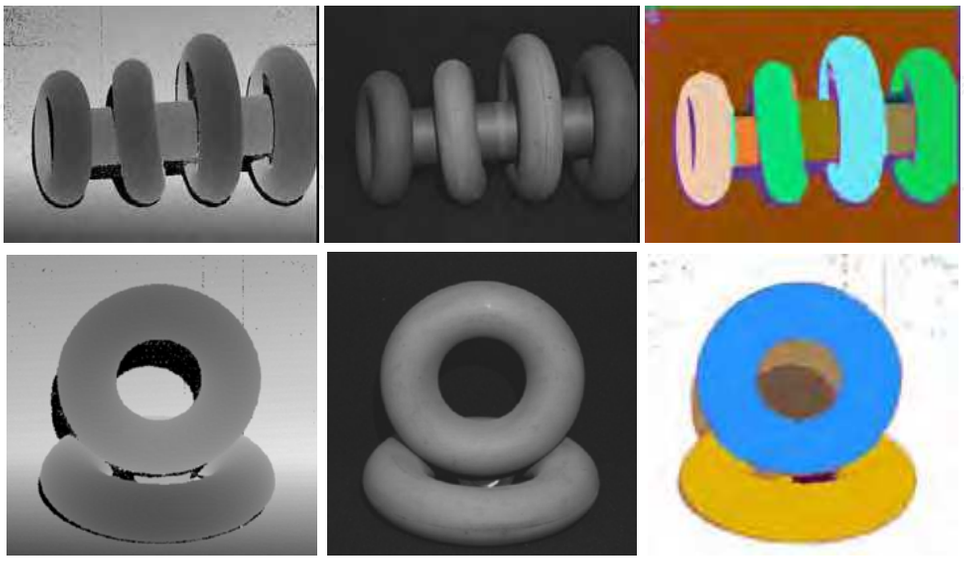

Fig. 9. Annuloid range, intensity and segmentation results images.

7. Conclusions

We proposed novel fast and accurate range segmentation method based on the combination of range & intensity profile modelling and curve-based region growing. A range profile is modelled using an adaptive simultaneous regression model. The recursive adaptive predictor uses spatial correlation from neighbouring data what results in improved robustness of the algorithm over rigid schemes, which are affected with outliers often present at the boundary of distinct shapes. A parallel implementation of the algorithm is straightforward, every image row and column can be processed independently by its dedicated processor. The region growing step is based on the cubic spline curve model. The algorithm performance is demonstrated on the set of test range images available on the University of South Florida web site. These preliminary test results of the algorithm are encouraging; the proposed method was mostly able to find objects present in all our experimental scenes with excellent border localization precision and outperformed the alternative segmenters. The proposed method is fast and numerically robust so it can be used in an on-line virtual reality acquisition system. However further work is still needed to replace current fixed region growing threshold with an adaptive threshold which could accommodate different types of range data, to test the performance on noisy laser data as well as on scenes with large number of curved faces.

8. Acknowledgements

This research was supported by the EC project no. FP6-507752 MUSCLE, grants No.A2075302, 1ET400750407 of the Grant Agency of the Academy of Sciences CR and partially by the MSMT grants 1M0572 DAR, 2C06019.

9. References

Besl P. J., Jain R. C., *Three-dimensional object recognition.* ACM Computing Surveys, 17, no.1, pp. 75-145, 1985.

Besl P. J., Jain R. C., *Segmentation Through Variable-Order Surface Fitting.* IEEE Transactions PAMI, Vol. 10, No.2, pp. 167-192, 1988.

Bock M. E., Guerra C., *Segmentation of range images through the integration of different strategies*, Vision, Modeling, and Visualization, pp. 27-33, 2001.

Chang Y. L., Li X., *Adaptive image region-growing*, IEEE Transaction on Image Processing, vol. 3, pp. 868–872, 1994.

Chu C., Aggarwal J. K., *The integration of image segmentation maps using region and edge information*, IEEE Transactions Pattern Analysis and Machine Intelligence, vol. 15, pp. 241–252, 1993.

Dubrawski A., Sawwa R., *Laserowe trójwymiarowe czujniki odleglości w nawigacji ruchomych robotów (3-D Laser Range Finders for Mobile Robots' Navigation)*, 5th National Conference on Robotics, Swieradow Zdroj, Poland 1996.

Flynn P. J., Jain A. K., *BONSAI: 3D Object Recognition Using Constrained Search.*, IEEE Transactions PAMI, Vol. 13, No. 10, pp. 1066-1075, 1991.

Forsyth D. A., Ponce J., *Computer Vision A Modern Approach*, Prentice Hall, Pearson Education, Inc., 2003.

Haddon J., Boyce J., *Image segmentation by unifying region and boundary information*, IEEE Transactions on Pattern Analysis and Machine Intelligence, Vol. 12, pp. 929-948, 1990.

Haindl M., Šimberová S., *Theory & Applications of Image Analysis*, chapter *A Multispectral Image Line Reconstruction Method*, pages 306--315, World Scientific Publishing Co., Singapore, 1992.

Haindl M., Žid P., *Range image segmentation by curve grouping*, In K. Dobrovodský, editor, Proceedings of the 7th International Workshop on Robotics in Alpe-Adria-Danube Region, pages 339--344, Bratislava, June 1998. ASCO Art.

Haralick R. M., Shapiro L. G., *Survey: Image segmentation techniques*, Computer Vision, Graphics, and Image Processing, vol. 29, pp. 100–132, 1985.

Hijjatoleslami S. A., Kittler J., *Region growing: A new approach*, IEEE Transaction on Image Processing, vol. 7, pp. 1079–1084, 1998.

Hoffman R. L., Jain A. K., *Segmentation and Classification of Range Images.*, IEEE Trans. PAMI, Vol. 9, No. 5, pp. 608-620, 1987.

Hoover A., Jean-Baptiste G., Jiang X. Y., Flynn P. J., Bunke H., Goldof D. B., Bowyer K., Eggert D. W., Fitzgibbon A., Fisher R. B., *An Experimental Comparison of Range Image Segmentation Algorithms.*, IEEE Trans. PAMI, 18, no.7, pp. 673-689, 1996a.

Hoover A., Jean-Baptiste G., Jiang X. Y., Flynn P. J., Bunke H., Goldof D. B., Bowyer K., Eggert D. W., Fitzgibbon A., Fisher R. B., *Range image segmentation comparison segmenter codes and results*, http://marathon.csee.usf.edu/range/seg-comp/results.html, 1996b.

Horn B. K. P., *Robot Vision*, MIT Press, 1986.

Internet: *OSU (MSU/WSU) Range Image Database*, http://sampl.eng.ohio-state.edu/~sampl/data/3DDB/RID/index.htm, 1999.

Jiang X. Y., Bunke H., *Fast Segmentation of Range Images into Planar Regions by Scan Line Grouping.*, Machine Vision and Applications, 7, no. 2, pp. 115-122, 1994.

Jiang X. Y., Bunke H., *Range image segmentation: Adaptive grouping of edges into regions.*, Asian Conference on Computer Vision, Hong Kong, 1998.

Jiang X., Bowyer K., Morioka Y., Hiura S., Sato K., Inokuchi S., Bock M. E., Guerra C., Loke R. E., du Buf J. M. H., *Some Further Results of Experimental Comparison of Range Image Segmentation Algorithms*, 15th International Conference on Pattern Recognition, Vol. 4, pp. 877-881, 2000.

Lee K. M., Meer P., Park R. H., *Robust Adaptive Segmentation of Range Images*, IEEE Transactions on Pattern Analysis and Machine Intelligence, Vol. 20, No. 2, pp. 200-205, 1998.

Loke R. E. and du Buf J. M. H., *Hierarchical 3D data segmentation by shape-based boundary refinement in an octree using orientation-adaptive filtering*, Tech. Report UALG-ISACS-TR03, 1998.

Dr McIvor A. M., Penman D. W. and Waltenberg P. T., *Simple Surface Segmentation.*, DICTA/IVCNZ97, Massey University, pp. 141-146, 1997.

Pal N. R., Pal S. K., *A review of image segmentation techniques*, Pattern Recognition, Vol 26, pp. 1277-1294, 1993.

Palmer P. L., Dabis H., Kittler J., *A performance measure for boundary detection algorithms*, Computer Vision and Image Understanding, vol. 63, pp. 476–494, 1996.

Pavlidis T., Liow Y. T., *Integrating region growing and edge detection*, IEEE Transactions Pattern Analysis and Machine Intelligence, vol. 12, pp. 225–233, 1990.

Powell M., Bowyer K., Jiang X., Bunke H., *Comparing curved-surface range image segmenters*, In {\em ICCV'98}, Bombay, 1998. IEEE.

Sinha S. S., Jain R., *Handbook of Pattern Recognition and Image Processing*, Wiley, New York, 1994.

Wilson R. and Spann M., *Image Segmentation and Uncertainty*, Research Studies Press Ltd., Letchworth, 1988.

Zhang X., Zhao D., *Range image segmentation via edges and critical points.*, Proc. SPIE, 2501, no. 3, pp. 1626-1637, 1995.

Vision Systems: Segmentation and Pattern Recognition

Edited by Goro Obinata and Ashish Dutta

ISBN 978-3-902613-05-9

Hard cover, 536 pages

Publisher I-Tech Education and Publishing

Published online 01, June, 2007

Published in print edition June, 2007

Research in computer vision has exponentially increased in the last two decades due to the availability of cheap cameras and fast processors. This increase has also been accompanied by a blurring of the boundaries between the different applications of vision, making it truly interdisciplinary. In this book we have attempted to put together state-of-the-art research and developments in segmentation and pattern recognition. The first nine chapters on segmentation deal with advanced algorithms and models, and various applications of segmentation in robot path planning, human face tracking, etc. The later chapters are devoted to pattern recognition and covers diverse topics ranging from biological image analysis, remote sensing, text recognition, advanced filter design for data analysis, etc.

InTech Europe
University Campus STeP Ri
Slavka Krautzeka 83/A
51000 Rijeka, Croatia
Phone: +385 (51) 770 447
Fax: +385 (51) 686 166
www.intechopen.com

InTech China
Unit 405, Office Block, Hotel Equatorial Shanghai
No.65, Yan An Road (West), Shanghai, 200040, China
中国上海市延安西路65号上海国际贵都大饭店办公楼405单元
Phone: +86-21-62489820
Fax: +86-21-62489821

IntechOpen